Assessment of Water Surface Reflectance and Optical Water Types Over Two Decades in Europe's Largest Artificial Lake: An Intercomparison of ESA and NASA Satellite Data

Gonçalo Rodrigues ⬤, Miguel Potes ⬤, and Maria João Costa

Abstract—This study focuses on comparing surface reflectances and optical water types (OWTs) obtained in Alqueva reservoir, located in the Alentejo region (Portugal), over a period of two decades (2003–2022) using four datasets: the moderate resolution imaging spectroradiometer (MODIS), the medium-resolution imaging spectrometer, the ocean and land color instrument aboard Sentinel-3, and the multispectral instrument aboard Sentinel-2. The MODIS instrument covers the entire study period and acts as the benchmark for intercomparing the surface reflectances obtained with the other three sensors. The classification of OWTs is based on differences in reflectance spectra, facilitating a qualitative assessment of water quality. This approach identified four distinct clusters, with two OWTs representing water with higher turbidity, facilitating the differentiation of reflectances associated with microalgae blooms and other phenomena such as runoff. However, when using MODIS, which covers only the central area of the reservoir, only three clusters were identified as the ideal number. Using 300 or 1000 m of spatial resolution, the Alqueva reservoir mostly exhibits high water transparency, associated with low surface reflectances for the majority of the time. Seasonal analysis revealed periods with the presence of microalgae in summer and autumn (SON), with a noticeable increase in the intensity and duration of these blooms in the SON period over the last ten years. This methodology enables the identification of advantages and disadvantages associated with the utilization of each sensor in large reservoirs and across extensive datasets.

Index Terms—Big data, microalgae blooms, multispectral satellite data, optical water types (OWTs), remote sensing monitoring, second simulation of a satellite signal in the solar spectrum, time-series.

I. INTRODUCTION

FRESHWATER is an essential resource that must be increasingly preserved for the future, especially considering the growing global population, the increasing water consumption, and the influence of climate change on precipitation patterns. With climate models anticipating more frequent and extended drought periods and heatwaves in various regions, such as Western Europe and the Mediterranean basin [1], [2], [3], [4], water reservoirs become essential for water storage. Satellite remote sensing plays a crucial role in monitoring water quality [5], [6], [7] because it allows for global coverage of reservoirs rather than the point-based monitoring typically associated with conventional methods. This global perspective is invaluable for understanding and managing water resources on a larger scale.

In a water reservoir, monitoring the evolution of water quality, including its spatial and temporal variations, as well as trends over decades, can greatly benefit from the integration of multiple sensors onboard satellites. In addition, when the goal is to monitor changes in water quality over two or more decades, it is anticipated that certain satellites might become obsolete while new ones are launched during that period [8]. To track these changes over time, a critical process involves intercomparing satellite data collected by the various sensors used over an extended duration [9]. A first step to characterize the evolution of water quality using empirical algorithms applied to water bodies involves the use of surface reflectance data from various optical sensors [10], [11], [12]. To obtain this surface reflectance, it is necessary to perform atmospheric correction that transforms top-of-atmosphere reflectance into surface reflectance by removing atmospheric interference. Institutions that provide satellite images, such as the European Space Agency (ESA) or the National Aeronautics and Space Administration (NASA), supply surface reflectance data as a product already corrected for atmospheric components [13], [14], [15], [16]. However, each atmospheric correction method used by different institutions may, inherently, differ from one to another. These differences can lead to variations in surface reflectance values at the same points, introducing a source of error when analyzing spatial and temporal variations in water quality using different sensors. To mitigate this variability introduced by distinct atmospheric correction methods and distinct atmospheric databases, it is

desirable to employ the same atmospheric correction method and input data for all the different sensors.

This approach helps to ensure consistency in the surface reflectance data, enabling more accurate and reliable assessments of water quality across various sensors. So, in this study, the same atmospheric correction code was applied to top-of-atmosphere images from various sensors applied in the largest artificial lake in Europe (Alqueva reservoir).

Alqueva reservoir experiences a well-defined water stratification period from April/May to September/October and exhibits eutrophic conditions in areas more susceptible to poor water quality [17]. However, in other areas, particularly larger and deeper sections, the trophic state is predominantly mesotrophic [18]. The very hot and dry summers lead to a significant increase in water temperature during the summer months, resulting in the formation of microalgae blooms or even cyanobacteria in the Alqueva reservoir [12], [19], [20]. The largest artificial lake in Europe had its gates closed in 2002. By early 2003, the accumulated water volume was sufficient to monitor water quality using satellite images with 300-m spatial resolution, such as those obtained from the medium-resolution imaging spectrometer (MERIS) instrument onboard ESA's Environmental satellite (Envisat). Consequently, from 2003 to the present, monitoring water quality parameters and their spatial and temporal variations has been achievable.

Optical water types (OWTs) represent a classification system that is employed to categorize qualitatively the water quality in water bodies. This is based on the unique characteristics of their reflectance spectra. The reflectance spectrum of a water body is influenced by its composition and the key features used to classify OWTs include the wavelength of peak reflectance, the steepness of slopes, and the overall magnitude of reflectance across different wavelengths. By analyzing these spectral features, it is possible to infer qualitative information about the water quality of a water body. An OWT classification can be easily used and analyzed by competent entities for the purposes of water quality monitoring. Furthermore, it can also be utilized in an alert system that monitors the onset of eutrophication or areas exhibiting a rapid deterioration of water quality.

In this study, surface reflectance data and OWTs from January 2003 to December 2022 were employed with the following key objectives.

1) Satellite Intercomparison of surface reflectances among the various sensors using a pixel-to-pixel comparison.
2) Identification of spatial and spectral variations among the different sensors, their application, and relevance for Alqueva reservoir.
3) Qualitative assessment of water quality through a comparison of the evolution of OWTs defined over two decades, assessing the significance of spectral and spatial resolution in the results obtained.

Water quality in Alqueva reservoir has been analyzed using both in situ measurements and laboratory data [18], [20], [21], [22], [23], [24], [25], [26], [27], [28], taken discreetly in space and time, as well as remote sensing data as supplementary observational data during selected periods [12], [29], [30], [31], [32].

Nevertheless, to our knowledge, this study represents the first complete analysis of water quality in this reservoir spanning over two decades using remote sensing data, in the period between January 2003 and December 2022.

Satellite missions, such as NASA's PACE (Plankton, Aerosol, Cloud, Ocean Ecosystem), will provide enhanced spectral resolution that could significantly improve our ability to monitor water quality, detect microalgae blooms, and identify the extent/duration of harmful algae blooms, particularly in large lakes, estuaries, or in the ocean. The methodologies discussed in this study, which focus on intercomparison across different sensors to ensure data continuity, will be crucial when integrating PACE data with existing datasets. This integration is essential for understanding current water quality and microalgae blooms, as well as tracking long-term trends to assess the impacts of climate change. By combining data from PACE with historical datasets, we can gain a more comprehensive understanding of the dynamics of aquatic ecosystems and the effects of climate change on water quality.

II. STUDY AREA AND DATA

A. Study Area

The Alqueva reservoir is the largest artificial lake in Portugal (see Fig. 1) and Western Europe with a surface area of 250 km^2, 4150 hm^3 of maximum storage capacity, and 3150 hm^3 of useful capacity. It follows the course of the Guadiana River located in the Alentejo region, south of Portugal, and constitutes the border between Portugal and Spain in the northern part of the reservoir. In February 2002, the gates of the dam were closed, marking the beginning of the reservoir's filling. By March 2003, Alqueva reached the quota of 136 m, and one year later, in April 2004, it reached 148 m, nearly 80% of its maximum capacity. The construction of the dam and the formation of the reservoir were designed for multiple purposes, including river flow regulation, hydroelectric power generation, and water supply for human consumption and irrigation. In a region with long periods of drought, the Alqueva reservoir has enabled the introduction of new crops and irrigation techniques, particularly focusing on olive groves, almond orchards, and vineyards.

In terms of climate, the eastern Alentejo region experiences significant irregularities in precipitation with limited rainfall during the summer and is characterized by a hot Mediterranean summer climate (Csa type, according to the Köppen climate classification). There are also years with extremely low precipitation, during which the Alqueva reservoir becomes essential for water supply to its communities [33].

B. Data Used

Satellite data from two decades, between January 2003 to December 2022, were used from various sensors: MERIS, Sentinel-3 ocean and land cover instrument (OLCI), Sentinel 2 multispectral instrument (MSI), as well as the moderate resolution imaging spectroradiometer (MODIS). The sensors used to monitor water
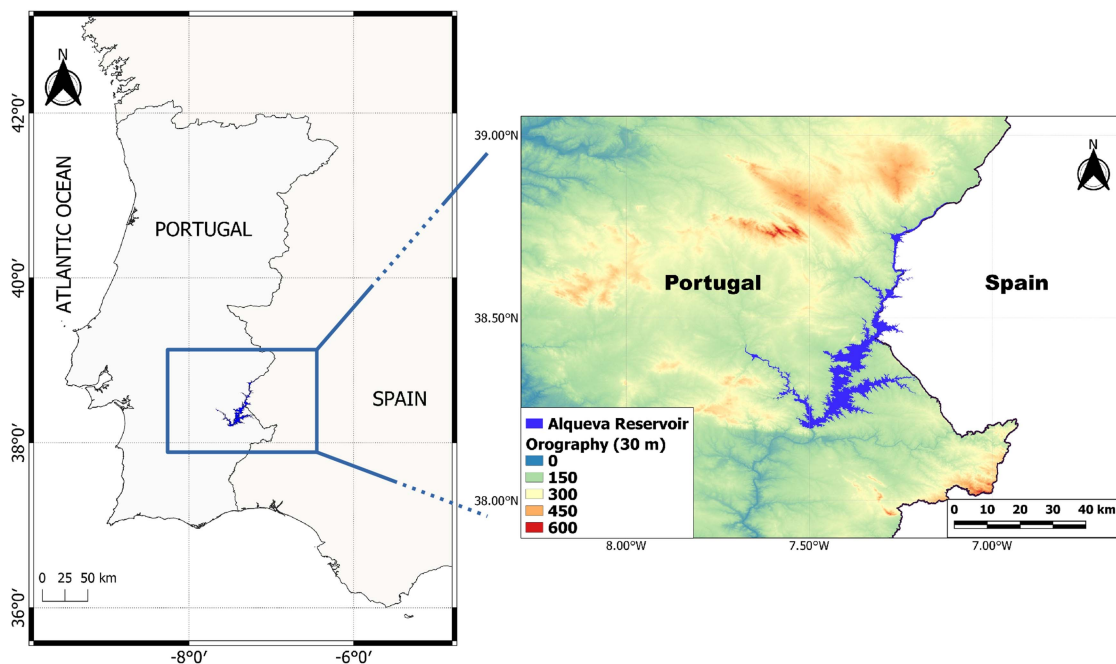
Fig. 1.   Location of the Alqueva reservoir, the study area, in Southeast Portugal.

TABLE I
BAND NUMBER, CENTRAL WAVELENGTH (NM), AND BANDWIDTH (NM) FOR EACH OF THE FOUR INSTRUMENTS USED IN THE WAVELENGTH RANGE 443–709 NM

OLCI (300 m)		MERIS (300 m)		MODIS (1000 m)		MSI (10, 20, 60 m)	
Band (Central λ)	Bandwidth (nm)	Band (Central λ)	Bandwidth (nm)	Band (Central λ)	Bandwidth (nm)	Band (Central λ)	Bandwidth (nm)
B3 (443)	10	B2 (443)	10	B9 (443)	10	B1 (443)	20
B4 (490)	10	B3 (490)	10	B10 (488)	10	B2 (493)	65
B5 (510)	10	B4 (510)	10	B11 (531)	10	-	-
B6 (560)	10	B5 (560)	10	B12 (551)	10	B3 (560)	35
B7 (620)	10	B6 (620)	10	-	-	-	-
B8 (665)	10	B7 (665)	10	B13 (667)	10	B4 (665)	30
B9 (674)	7.5	-	-	-	-	-	-
B10 (681)	7.5	B8 (681)	7.5	B14 (678)	10	-	-
B11 (709)	10	B9 (709)	10	-	-	B5 (704)	14

The bands marked in gray are not used in this work.

quality in lakes have different spatial, temporal, and spectral resolutions. MODIS [34] is a remote sensing instrument on board two NASA satellites, MODIS Terra and MODIS Aqua. One of the key differences between these two sensors is their overpass time. MODIS Terra passes around 10:30 A.M. and it is chosen because its overpass time is closer to that of the other sensors used in this work.

The MODIS dataset used in this research consists of Level 1B calibrated radiance data, specifically the product code MOD021KM. The DOI for this dataset is 10.5067/MODIS/MOD021KM.061. The spectral bands used are indicated in Table I and present a spatial resolution of 1 km². In the article, the term MODIS represents MODIS Terra data. MERIS [35] is one of ten sensors deployed on board the ESA's

polar-orbiting environmental research satellite (Envisat-1) in March 2002. MERIS data in Full resolution mode present a spatial resolution of 300 m. MERIS spectral bands used are indicated in Table I. Sentinel-3A is an ESA Earth observation satellite dedicated to oceanography and inland waters launched on 16 February 2016 and built as part of the Copernicus program. ESA's Sentinel-3B satellite was launched on April 25, 2018.

One of its key instruments is the OLCI, with one overpass every day over the Alqueva reservoir. MERIS and OLCI are MSIs, specifically designed for monitoring waterbodies and oceans, offering numerous spectral bands with narrow bandwidths, suitable for observing phenomena such as microalgae blooms and turbid waters. The use of these ESA sensors allows to have a
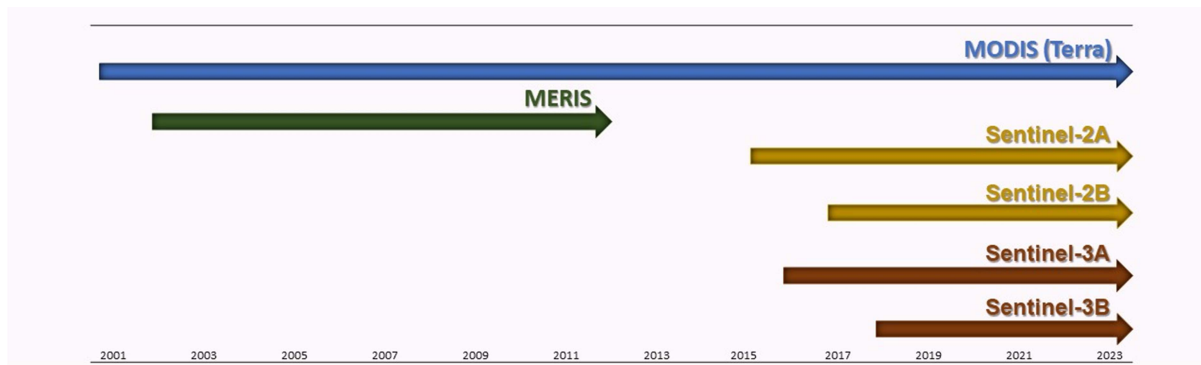
Fig. 2.　Operational period for each sensor used.

temporal coverage of 20 years, from 2003 to the present, except for the period between April 2012 and March 2016. During the latter period, MODIS data were used, and from July 2015 onwards, data from the high-resolution MSI), onboard Sentinel-2A and Sentinel-2B, were also incorporated into the study. These twin polar-orbiting satellites allow for a high revisit time of two–three days for Alqueva reservoir, since July 2017, with high spatial resolution ranging between 10 and 60 m. The temporal coverage of each of the sensors used is presented in Fig. 2 and the bands used in this work, with their central wavelengths and bandwidths, are summarized in Table I. The most suitable MODIS bands for water quality monitoring have a spatial resolution of 1000 m (suitable mainly for very large reservoirs). On the other hand, the Sentinel-2 MSI instrument offers an excellent spatial resolution suitable even for small reservoirs (resolution ranging from 10 to 60 m). Although its spectral bands are not optimal for microalgae detection in comparison to those of other instruments analyzed in this study, and it was primarily designed for terrestrial applications, the MSI's high spatial resolution allows for the detection and monitoring of potentially harmful algae blooms and can be used in small inlets of the reservoir where other instruments with a 300 m spatial resolution, such as OLCI, cannot be used [36]. However, MODIS was launched in December 1999 on the polar orbiting NASA Earth Observing System, later renamed Terra and Aqua, allowing it to provide coverage spanning over two decades, unlike the instrument MSI, which was launched in 2015 (see Fig. 2). MERIS and OLCI data in full resolution mode presents a spatial resolution of 300 m.

III. METHODS

In this section, the methods applied to data over Alqueva reservoir in the period 2003–2022 are presented. Sensors from both ESA and NASA were utilized, with distinct temporal, spatial, and spectral resolutions. To establish a comparison between surface reflectances obtained from different sensors, several intermediary steps were undertaken. These intermediary steps and the entire methodology are presented in Fig. 3.

A. Preprocessing and Atmospheric Correction

The preprocessing of top of the atmosphere (TOA) images, including reading, reprojecting (Geodetic CRS: WGS 84), subsetting for the study area, and extraction of the bands and products of interest, was performed on the SNAP toolbox (Sentinel Application Platform, http://step.esa.int/main/toolboxes/snap/, last accessed on 1 August 2023), using the batch processing tool for optimization and faster processing. Sentinel-2 MSI reflectances at 10, 20, and 60 m spatial resolution were resampled to 300 m pixel size using block averaging as a downsampling method prior to atmospheric correction to match the spatial resolution of the OLCI and MERIS sensors. In addition to TOA reflectances for each of the analyzed bands in this study (see Table I), geometrical products were also exported to be used in the atmospheric correction scheme, such as the view zenith angle (VZA), solar zenith angle (SZA), view azimuth angle, and solar azimuth angle. Normalized difference water index (NDWI) utilizes the green and near-infrared (NIR) bands for masking, delineating water features, i.e., excluding nonwater surface reflectances. To determine the optimal NDWI threshold for each sensor (MSI, OLCI, MERIS, and MODIS), a systematic approach was employed. Starting with an NDWI value of 0.0, the threshold was gradually increased until only pixels corresponding to pure water remained. This process was guided by two criteria: 1) under clear sky conditions, the number of pixels classified as water within the reservoir should remain relatively stable over time; and 2) K-means clustering was used to identify distinct spectral classes within the imagery, ensuring that no clusters represented nonwater features such as soil, vegetation, or mixed pixels. Finally, a visual inspection of the images using the red, green, and blue bands was conducted for each sensor after applying the NDWI filter to confirm that intense microalgae blooms, runoff, and sunglint were effectively captured or filtered, respectively. Images with sunglint were excluded rather than corrected, as the region has a large number of cloudless days during the months when this phenomenon occurs (April to August).

The performance of atmospheric correction decreases with a higher VZA, SZA, and aerosol optical thickness at 550 nm
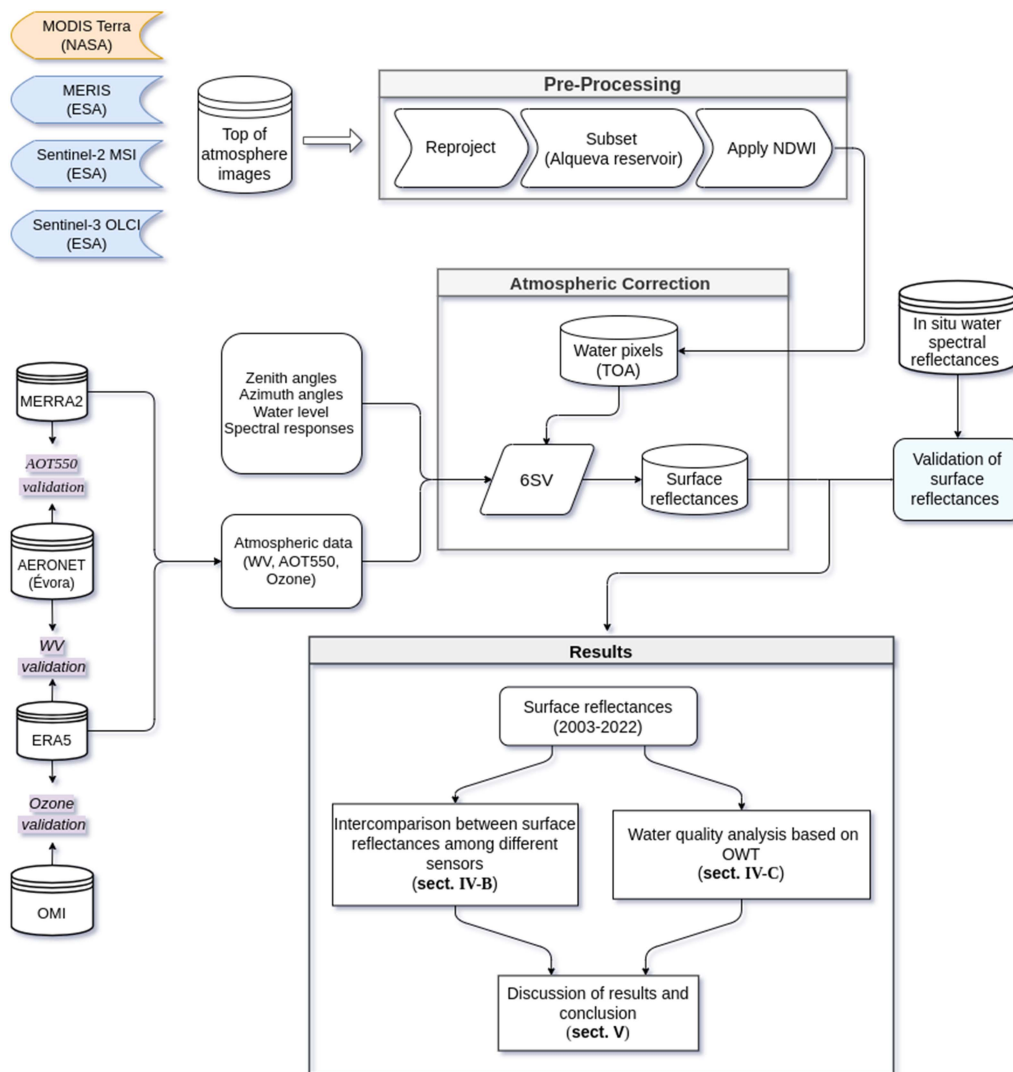
Fig. 3.   Flowchart showing the methodology developed.

(AOT550). For this reason, filters were implemented to exclude days analyzed by satellite remote sensing based on the following conditions: VZA > 30° and AOT550 > 0.150. The data analysis showed that very few days (no days) were identified over the Alqueva reservoir with VZA greater than 30° for MERIS (MSI). However, for OLCI and MODIS instruments, several days with VZA greater than 30° were observed. While some other authors apply a significantly higher VZA filter [37], [38], [39] in this study, the threshold of 30° was adopted to minimize the differences in VZA among the various instruments used, thus avoiding variations in atmospheric correction performance. The SZAs did not exceed the recommended exclusion values in the literature, i.e., the values consistently remain below 70° and 75° [38], [39], peaking around the end of December, reaching approximately 65° in the Alqueva reservoir. In addition, these angles showed similar values for the different sensors since their overpasses are close in time.

The analysis of water surface properties using remote sensing techniques requires the removal of atmospheric effects resulting

from absorption and scattering processes. In clear sky conditions, the main atmospheric effects that need correction are connected with aerosols, water vapor (WV), and ozone, which primarily impact the visible spectral region, harnessed to estimate water quality parameters. The Évora Atmospheric Sciences Observatory (Portugal) has been consistently measuring WV and aerosol optical thickness (AOT) data, constituting a site included in the Aerosol Robotic Network (AERONET) [40], [41]. However, these measurements do not cover the entire study period and, consequently, were not used to perform the atmospheric correction here.

The goal is to establish a consistent data source for ozone, WV, and AOT550 to avoid potential discontinuities that could result from using different sources for each of these atmospheric compounds. For this reason, ozone and WV data used in the atmospheric correction were obtained from the European Centre for Medium-Range Weather Forecasts as part of the ERA5 database. ERA5 is a high-resolution global climate dataset (1-h temporal) with a $0.25° \times 0.25°$ grid (reanalysis product) that

provides detailed information about Earth's climate over eight decades now (from 1940 to present). The AOT550 data used were sourced from Modern-Era Retrospective Analysis for Research and Applications, Second Edition (MERRA2), a dataset produced by NASA. MERRA2 was chosen due to its high spatial resolution ($0.5° \times 0.625°$ grid), appropriate temporal resolution (hourly data), and rigorous validation process [42]. The accuracy of these products, as well as the uncertainty that may be introduced by these two types of databases, was evaluated prior to their utilization, for the study area considered here through comparison with AERONET data from the Évora site, as well as with the ozone monitoring instrument (OMI) data for ozone (see Section IV-A).

The atmospheric correction procedure was applied to the TOA images of the four sensors considered to obtain surface spectral reflectances. The second simulation of a satellite signal in the solar spectrum (6SV) was the radiative transfer code adopted because it has been successfully applied before and validated for some of the sensors used in this study [19], [31], [32]. Furthermore, in our study area, there are periods with very clean water and thus very low spectral reflectance, which requires a very accurate correction to avoid meaningless results of null or negative spectral reflectance values. This issue was found only in a few cases corresponding to high aerosol loads in the atmosphere.

The surface spectral reflectances obtained from 6SV were validated through comparison with water spectral reflectances measured with a portable spectroradiometer FieldSpec UV/VNIR (ASD, Inc., Bouler, CO, USA) (see Section IV-A). The FieldSpec UV/VNIR is a hyperspectral radiometer with a spectral range of 325–1075 nm and a spectral resolution of 1 nm. In situ surface reflectances were collected under clear sky conditions and were only carried out in locations with high depth, in order to allow for a correct measurement (at moorings or from a boat far from the shore), and were made with the 10° field-of-view. The surface reflectance is calculated as the ratio between the energy leaving the sample by reflection and the energy incident on the sample (obtained from the white reference panel). This is done by measuring the energy leaving the sample by reflection in the water immediately after the measurement on the white reference, ensuring that the illumination for the lake and white reference is very similar. In situ values were obtained by averaging 25 spectra, selected to represent the typical surface reflectance for each observation point. More details about the FieldSpec UV/VNIR (ASD, Inc.) and measurements at Alqueva can be found in [28] and [43].

B. Intercomparison Between the Four Sensors

The pixel-to-pixel technique was adopted to compare surface reflectances from different remote sensing sensors, directly comparing colocated pixels. For the intercomparison between the MODIS sensor with the other instruments, the MSI data were initially resampled to a 300 m resolution. To ensure a more equitable comparison between satellites with different spatial resolutions, particularly when comparing MODIS (1000

m resolution) with the ESA sensors, this involved calculating the average of the nine nearest water pixels. This approach resulted in a comparison that closely approximated the sensors, with spatial resolutions of 1000 m for MODIS and 900 m for MERIS, OLCI, and MSI. Only cases where all nine higher resolution pixels were fully contained within the MODIS pixel were considered, ensuring that the distance between pixels did not exceed 600 m. In addition, the closest pixel of higher resolution satellites (300 m) was compared with the MODIS pixel (1000 m) and related this to the results for 900 m $\times$ 1000 m. The purpose of this comparison is to illustrate the statistical improvement achieved by reducing the difference in spatial resolution, particularly in the broader areas of the reservoir (pixels where the MODIS instrument identifies water pixels).

In addition to the intercomparison of surface reflectances, the OWTs obtained using each of the sensors were also compared. A clustering method was applied to surface spectral reflectances collected from 2003 to 2022. This method grouped spectra with different water quality characteristics, indicated by variations in both amplitude and reflectance curve shape. The clustering technique utilized was the K-means method, a robust approach suitable for handling large datasets [44], [45], [46]. Prior to applying the clustering method, a preliminary step was implemented for normalizing each of the spectra [47]. Normalization ensured that the absorption characteristics of the water constituents had a more significant influence on the grouping process. Without this normalization, the resulting groups representing different OWTs would be primarily based on the range of reflectance values rather than the shape of the spectral curve. Based on information derived from the "silhouette width" [48], some of the spectra and OWT assignments were excluded. The silhouette index assesses how effectively each spectrum is assigned to its respective cluster, with a range between -1 and 1. Values closer to 1 indicate more accurate assignments, while a value of 0 suggests that the spectrum falls on the boundary between two or more clusters. In this study, all spectra with a silhouette width lower than 0.05 were excluded. This index also allows the exclusion of pixels at the land–water boundary, which may have passed through the NDWI filter. In other words, it helps to exclude pixels that don't fit into purely "water" spectra.

In order to ascertain the optimal number of clusters for each instrument, the silhouette width was employed. The k-means clustering method was performed with the number of clusters varying from 3 to 9, with the average silhouette width calculated for each iteration. The maximum value of this index allows us to identify the optimal number of clusters. This suggests that the spectra within a cluster are more similar to each other than to those of other clusters, indicating a greater spectral distinction between the groups. Once the optimal number of clusters for each instrument had been determined, the mean spectrum for each cluster was calculated in order to characterize the different types of OWTs. Although the median was also calculated, the differences between the mean and the median were found to be insignificant, indicating that both measures can

be used to represent the clusters in a similar way in this case. Finally, the OWTs were ordered by the amplitude of surface reflectances, with OWT1 being characteristic of less turbid water.

The OLCI and MERIS sensors share the same central wavelength and bandwidth within the wavelength range from 490 to 709 nm, except for the 673.75 nm wavelength, which is unique to the OLCI sensor (see Table I). Since OLCI follows the same conceptual design as MERIS, these sensors exhibit very similar characteristics. The data from OLCI and MERIS were analyzed together before applying the K-means method. The resulting groups of OWTs are referred to as OWT$_{\text{MER\_OLCI}}$ throughout the document. OWTs were also obtained for the MODIS sensor (OWT$_{\text{MODIS}}$) using specific bands (B10, B12, B13, and B14 for MODIS) and B2–B5 for MSI. The OWTs for the MSI sensor (OWT$_{\text{MSI}}$) were determined by similarity to the average clusters established by the MERIS and OLCI sequence, denoted as OWT$_{\text{MER\_OLCI}}$. Given that the MERIS-OLCI series at a 300 m resolution spans approximately 16 years, capturing diverse optical conditions such as periods of better water quality, microalgae blooms, and intense precipitation events leading to runoff into the reservoir (notably in the initial months of 2010, and December 2022), it is considered a suitable and robust reference series for other sensors with more limited databases. Euclidean distance was employed as the similarity measure, taking into account the sensitivity of Euclidean distance to the data scale. The comparison involved normalized spectra from both MSI and the reference clusters (OWT$_{\text{MER\_OLCI}}$) in order to mitigate the influence of scale on assigning the closest cluster to each of the MSI spectra.

To compare the two long database used in this study defined by OWT$_{\text{MER\_OLCI}}$ and OWT$_{\text{MODIS}}$, contingency tables and concordance proportions were used. The agreement ratio was calculated by dividing the number of events with matching OWT assignments for two pairs of sensors by the total number of events. Temporal variations of OWTs from each sensor were analyzed seasonally, considering the winter (DJF), spring (MAM), summer (JJA), and autumn (SON) seasons.

IV. RESULTS

A. Atmospheric Correction

The use of satellite data to study the water surface requires the application of an atmospheric correction methodology that removes the effects of the atmosphere and provides spectra representing the water mass. Before applying the 6SV code to each pixel for all clear-sky days (TOA images), between 2003 and 2022, validation of ozone, WV, and AOT550 was performed to assess the quality of these products in the Alqueva reservoir. AOT550 from MERRA-2 and WV obtained from ERA5 for the region of study were compared with AERONET data from Évora station using the period 2010–2022 for validation purposes (see Fig. 9). ERA5 ozone is compared with measurements obtained from OMI instrument is also provided

in the AERONET data files. Of the three atmospheric compounds, AOT550 exhibits the largest deviation from observations. Therefore, the validation was divided into two time periods, 10:30 and 11:30, in order to assess differences in validation for each of these time periods used in atmospheric correction.

The comparison between ERA5 and observation data shows a very good agreement with correlations exceeding 0.95 and MAPE of only 3% and 13% for ozone and WV, respectively (see Fig. 9). AOT presents correlation coefficients greater than 0.8, and data present more dispersion and higher absolute errors with respect to water vapor and ozone. Nevertheless, the greater dispersion is outside the range used in this study, i.e., for AOT550 greater than 0.15. It is noteworthy that the statistical results are very similar between 10:30 and 11:30, which is a positive factor as it avoids additional sources of discontinuity caused by the time difference between satellite images.

The 6SV atmospheric correction method has previously been utilized and validated for the Alqueva reservoir with the MERIS, MSI, and OLCI instruments [19], [31], [32]. The validation for the MODIS instrument is presented in Fig. 4 for the bands that coincide with ESA sensors between the wavelengths of 488 and 678 nm, where MODIS surface reflectances obtained from the 6SV code were compared with measured surface reflectances. For each of the 27 in situ measurements used, 25 surface reflectance spectra were obtained, and the average of these spectra was calculated. To validate each spectral band, the MODIS spectral response function was applied to the in situ reflectances.

The satellite-derived water reflectances using the 6SV method tend to overestimate the measured water reflectance, suggesting a positive bias. It is noted that MODIS tends to overestimate surface reflectance data, with the bias values closely aligned with the MAE, except for the green region (551 nm), and a few data points falling below the $y = x$ line. The green band (551 nm) is pivotal for monitoring temporal changes in water biomass and the emergence/recession of algal blooms. Through the 6SV method, this band exhibits very good statistical indicators: a correlation almost reaching 1 ($r = 0.95$), minimal associated errors (MAPE of 18%), and most points nearly aligning with the ideal $y = x$ line. For the remaining three bands, despite the MAE being just over 0.005 (a low value), the error is relatively significant in percentage terms, ranging from 40% to 58% in MAPE. This is partly due to the consistently low reflectance values in the Alqueva reservoir (higher errors in percentage terms arise from very low reflectance values). The correlation between the measured and satellite-derived water reflectance is high/very high, except for the blue band (488 nm), which is still acceptable ($r = 0.74$).

B. Intercomparison Between Surface Reflectances From Different Sensors

MODIS is the only sensor that covers the entire period analyzed and was compared with the average of the nine nearby pixels of the 300 m resolution MERIS, OLCI, and MSI data.
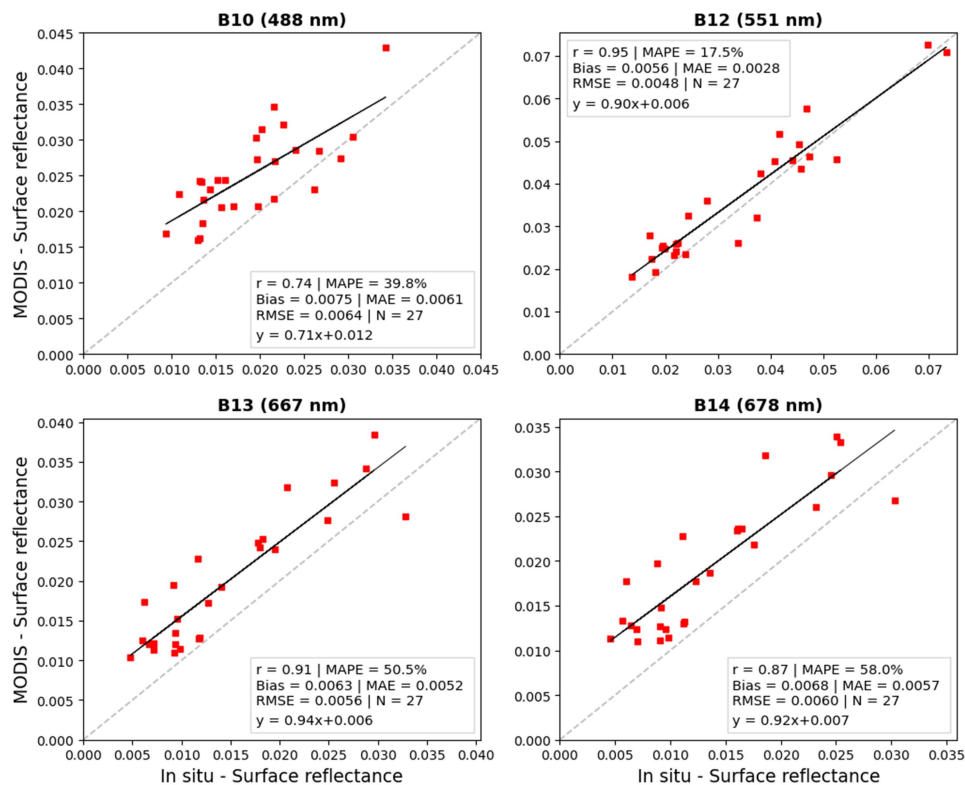
Fig. 4. Comparison between in situ and MODIS reflectances after atmospheric correction using the bands employed in this study. The dashed line represents the equation $y = x$.

For coinciding days and pixels, surface reflectances were compared for each band (see Table II). The difference in comparing 300 m × 1000 m and 900 m × 1000 m aims to demonstrate not only the improvement in statistical indices with less spatial difference between sensors but also to quantify spatial variations in surface reflectances.

There is a slight improvement in the statistical results when using a spatial coverage as similar as possible between sensors (900 and 1000 m) compared to using the nearest point. However, this improvement is quite modest, indicating limited heterogeneity in water quality as represented by surface reflectances. For a more equitable intercomparison, it is advisable to give greater weight to the 900 m resolution as it allows for comparing sensors at similar spatial resolutions. In the intercomparison between sensors, there is a strong agreement for the green band, specifically for the 551 nm of MODIS and 560 nm of the other sensors. Correlation coefficients (r) are equal to or greater than 0.96, and MAE values are below 11%. Large errors, significantly exceeding the mean absolute errors, are not commonly observed, as suggested by the proximity between the mean absolute percentage error (MAPE) and root mean square error (RMSE), both expressed as percentages. In general, errors obtained from the comparisons to the MODIS instrument result in underestimation (negative bias). For the wavelengths 667 and 678 nm, this bias is nearly systematic, with MAE almost equal to the bias in absolute values. The exception is observed for the blue band in the MERIS and MODIS comparison and the green band in the

OLCI versus MODIS comparison, where there is a slight underestimation compared to MODIS, with a bias of only 0.001 in both cases.

The statistical errors between the three ESA instruments and MODIS, using similar resolutions (900 versus 1000 m), have MAPE below 25%, except for the 681 nm band (OLCI), with a MAPE of 29%.

In Fig. 5, the intercomparison between the Sentinel-2 MSI sensor and the Sentinel-3 OLCI sensor is presented, with an equivalent resolution of 300 m (degrading the MSI of 10/20/60 m spatial resolution).

There is a very good statistical agreement between adjacent pixels captured by the MSI and OLCI instruments across all analyzed bands. Once again, the green wavelength band at 560 nm exhibited a correlation close to 1, low deviations, low MAPE, and data points closely aligned with the ideal condition $y = x$. While there was no systematic deviation for higher wavelengths (bottom subplots in Fig. 5), the blue (490 nm) and green (590 nm) bands showed that OLCI tended to overestimate compared to the MSI instrument. The positive bias values were very close to the MAE to these two bands.

C. Water Quality Analysis Based on OWT

1) Definition of OWTs: All water pixels were included to group spectra with similar characteristics within each of the

TABLE II
STATISTICAL ANALYSIS, COMPARING THE MODIS BANDS USED IN THIS ARTICLE WITH THE CLOSEST BANDS FOR MERIS, OLCI, AND MSI

|		r	Bias	MAE	MAPE (%)	NRMSE (%)	$Y = mx + b$	N
		MODIS (488 nm)						
MERIS (490 nm)	300 m	0.87	0.001	0.0028	13.9	17.4	$Y = 0.954x + 0.002$	1013
	900 m	0.88	0.0010	0.0027	13.6	16.9	$Y = 0.954x + 0.002$	
OLCI (490 nm)	300 m	0.07	-0.0027	0.0035	13.3	17.3	$Y = 0.073x + 0.0005$	646
	900 m	0.88	-0.0027	0.0033	12.8	16.7	$Y = 0.875x + 0.0005$	
MSI (493 nm)	300 m	0.87	-0.005	0.0051	19.8	24.6	$Y = 0.752x + 0.0014$	508
	900 m	0.87	-0.0049	0.0050	19.3	24.1	$Y = 0.751x + 0.0015$	
		MODIS (551 nm)						
MERIS (560 nm)	300 m	0.98	-0.0018	0.0032	11.4	12.9	$Y = 1.1x - 0.0049$	1013
	900 m	0.98	-0.0018	0.0031	10.9	12.3	$Y = 1.1x - 0.0049$	
OLCI (560 nm)	300 m	0.95	0.0009	0.0037	11.1	14.3	$Y = 1.1x - 0.0025$	646
	900 m	0.96	0.0010	0.0035	10.2	13.5	$Y = 1.1x - 0.0025$	
MSI (560 nm)	300 m	0.95	-0.0026	0.0035	11.4	15.1	$Y = 0.946x - 0.0009$	508
	900 m	0.96	-0.0025	0.0032	10.6	14.2	$Y = 0.943x - 0.0007$	
		MODIS (667 nm)						
MERIS (665 nm)	300 m	0.90	-0.0035	0.0040	20.5	25.4	$Y = 0.896x - 0.0014$	1013
	900 m	0.92	-0.0034	0.0038	19.4	24.0	$Y = 0.904x - 0.0015$	
OLCI (665 nm)	300 m	0.89	-0.0049	0.0054	26.5	34.3	$Y = 0.907x - 0.003$	646
	900 m	0.90	-0.0048	0.0051	24.8	32.7	$Y = 0.912x - 0.003$	
MSI (665 nm)	300 m	0.82	-0.0045	0.0047	24.3	34.1	$Y = 0.625x + 0.0023$	508
	900 m	0.84	-0.0043	0.0045	23.1	32.9	$Y = 0.621x + 0.0025$	
		MODIS (678 nm)						
MERIS (681 nm)	300 m	0.89	-0.0042	0.0045	23.9	28.6	$Y = 0.86x - 0.0015$	1013
	900 m	0.91	-0.0041	0.0043	22.8	27.3	$Y = 0.869x - 0.0016$	
OLCI (681 nm)	300 m	0.88	-0.0057	0.0060	30.1	38	$Y = 0.891x - 0.0036$	646
	900 m	0.89	-0.0056	0.0058	28.8	36.5	$Y = 0.898x - 0.0036$	
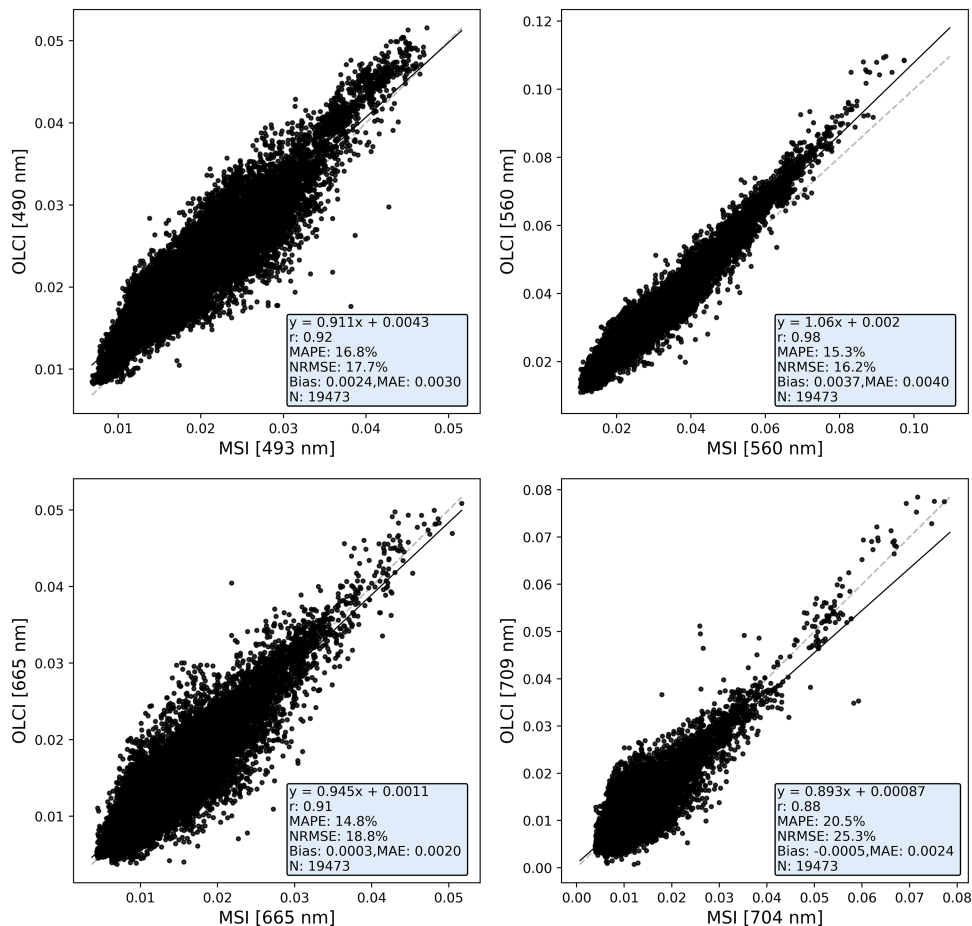
Fig. 5.　Statistical analysis comparing the MSI bands used in this article with the corresponding bands for OLCI (300 m spatial resolution). The dashed line represents the line $y = x$.
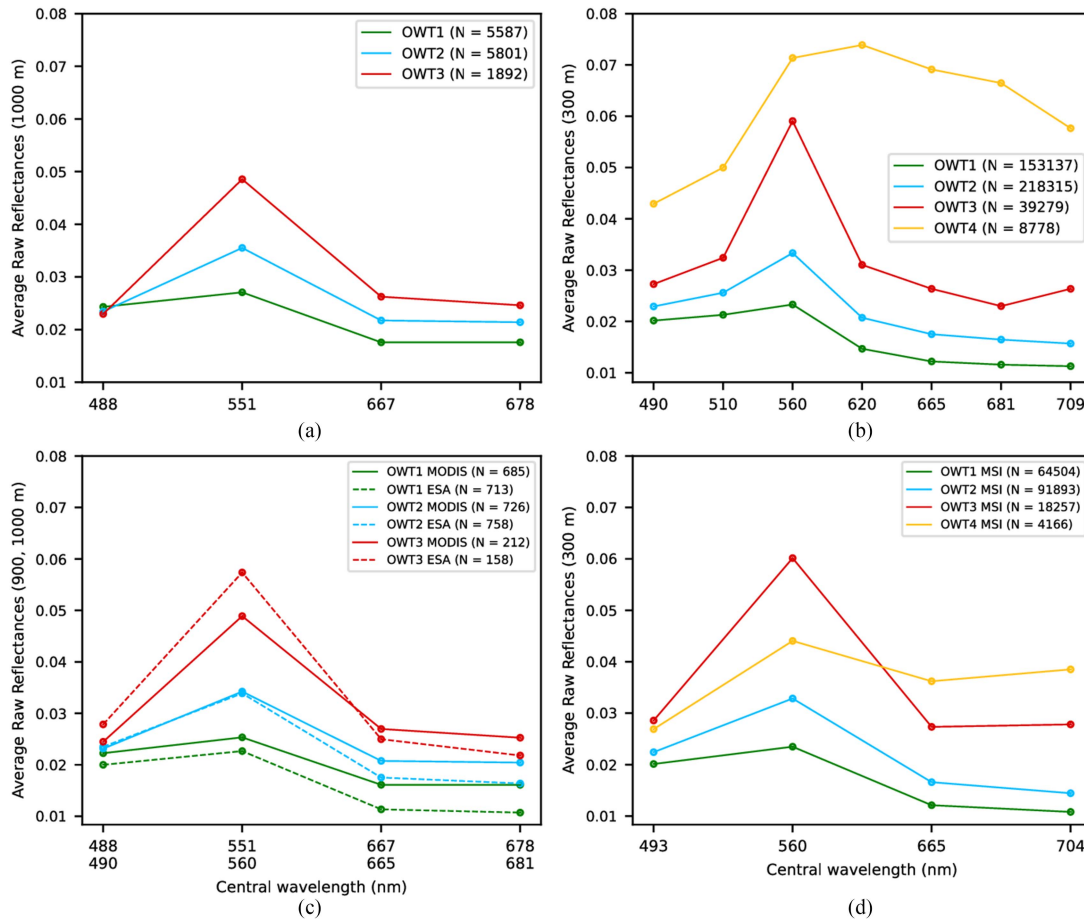
Fig. 6. (a) Mean raw reflectances for each cluster using the long time series with the MODIS instrument (top left). (b) MERIS series complemented by OLCI (top right). (c) Comparison between OWT_{MODIS} (1000 m) and OWT_{MER_OLCI} (resampled to 900 m) in bottom left. (d) Mean raw reflectances with OWT_{MSI} using the Euclidean distance (bottom right).

clusters. This methodology aims to obtain different water quality groups over the 20 years analyzed, and for this purpose, K-means clustering method (see Section III-B) was applied to the following groups of surface reflectances.

1) Reflectance spectra from MODIS (Full resolution mode) with a 1000 m of spatial resolution, covering the whole period. The selected wavelengths were 488, 551, 667, and 678 nm.

2) Reflectance spectra from MERIS and OLCI instruments with a 300 m resolution, however with a gap between April 2012 and March 2016. The selected wavelengths ranged from 490 to 709 nm, covering the spectrum between band B4 and band B11 (except B9) of the OLCI instrument, and from band B3 to band B9 for the MERIS instrument.

3) For a direct comparison between the OWT_{MER_OLCI} and OWT_{MODIS} with a similar spatial resolution (900 m versus 1000 m), we first computed the average of the nine OLCI and MERIS pixels before applying the K-means method. In addition, we utilized only the OLCI and MERIS bands that correspond to those in MODIS.

Different OWTs were assigned based on the remote sensing sensor, the spectral bands used, and the spatial resolution (see Fig. 6). The average raw reflectance for each of the OWTs described in point 1) is presented in the first subplot. The assignment of OWTs using MERIS and OLCI data, considering conditions 2) is shown in the second subplot. In the direct comparison between the assignment of OWTs from the MODIS sensor [condition 1)] and the OLCI and MERIS sensors [condition 3)], the average reflectance spectrum is shown in the third subplot. Finally, the last subplot (bottom right) displays the average raw reflectance for the MSI instrument, determined using the Euclidean method as a measure of similarity to the average clusters defined by the OWT_{MER_OLCI}.

The clusters were obtained based on normalized reflectances, as explained in Section III-B. Fig. 10 shows the average normalized reflectances of the OWT_{MER_OLCI} reference series for each of the cluster groups.

The analysis of the 20-year period shows that for a 300 m resolution in the Alqueva reservoir, the most effective approach is to use four clusters to distinguish different water quality groups based on reflectance spectra. However, after degrading the resolution to 900 m or using MODIS in full resolution

		MERIS_OLCI			
		OWT1	OWT2	OWT3	
MODIS	OWT1	505	173	0	74,5%
	OWT2	179	479	54	67,3%
	OWT3	7	74	126	60,9%
		73,1%	66,0%	70,0%	

Gray fields represent perfect agreement between sensors, meaning they have the same OWT assigned.

mode (1000 m), the ideal approach will be to use only three clusters. OWT1, in green, represents pixels with the best water quality, characterized by low surface reflectance. OWT2, in blue, represents pixels with water exhibiting higher turbidity compared to OWT1 but still without very high reflectance. The OWT3, represented in red color, is associated with a significant increase in the green band and is primarily related to microalgae blooms that occur with rising water temperatures in the reservoir between June and October. The OWT4 (yellow color) indicates areas with very turbid water due to runoff following periods of intense and persistent precipitation. It is only present with the use of 300 m resolution images, i.e., not identified with the MODIS sensor. This suggests that the effects of extreme precipitation events were mainly identified in narrower areas, which are more susceptible to rapid changes in water quality within the reservoir. Note that for all sensors used and at different spatial resolutions (300, 900, 1000 m), predominantly low surface reflectances are obtained, meaning a high assignment to cluster OWT1 and cluster OWT2, with average reflectances below 0.03 for these two clusters across the spectrum, except for the green wavelength (560 nm) for OWT2, where it may exhibit slightly higher reflectance values. Considering the OWT_{MER_OLCI} (300 m), 89% of the pixels are assigned to clusters representing better water quality (OWT1 + OWT2). Among these, 37% are assigned to cluster OWT1 with very low surface reflectances and a very subtle slope between the blue band (510 nm) and the green band (560 nm), indicating low or very low concentrations of chlorophyll-a and water with high transparency. Of the remaining 11% assigned, 9% were assigned to cluster OWT3, and only 2% to cluster OWT4 [see Fig. 6(b)]. The average raw reflectances of MSI are similar to the reference series (OWT_{MER_OLCI}) for all clusters, except for the cluster representing turbid water due to phenomena such as runoff (OWT4). This discrepancy in OWT4 may be attributed not only to the limited bands of MSI (and its larger bandwidths) but also to the fact that during the period 2015–2022, there were fewer runoff events, much less significant, for example, than those observed in the winter of 2009–2010.

2) Comparison of OWTs From Different Sensors: For a direct comparison, OWTs were obtained using the OLCI and MERIS wavelengths coinciding with MODIS. The obtained OWT_{MER_OLCI} were compared pixel by pixel with OWT_{MODIS}. For OWT_{MODIS}, only the wavelengths closest to the OLCI and MERIS wavelengths were considered, that is, using the bands B10 (488 nm), B12 (551 nm), B13 (667 nm), and B14 (678 nm). In Table III, a comparison is made between the different sensors using a contingency table.

In the comparison between OWT_{MODIS} and OWT_{MER_OLCI}, an average concordance of 70% is observed in the assignment of OWTs, despite some variation in concordance for different OWTs. When MODIS assigns OWT3 (representing the worst water quality), OWT_{MER_OLCI} assigns the same category in 61% of the instances, this being the combination of OWTs with the lowest agreement between the two series. This implies that if only MODIS data were utilized in the analysis, in scenarios where MODIS attributed OWT3, there would be at least a 61% probability that employing OWT_{MER_OLCI} would yield the same OWT attribution for the same area. On the other hand, there is higher concordance when the OWT3 assignment comes from OWT_{MER_OLCI}, in this case, there is agreement in 70% of the cases. There is a notably strong concordance between the two OWT series in the attribution of the cluster representing the best water quality, particularly when OWT1 is assigned for OWT_{MODIS}, showing a match in 75% of instances. When there's a degradation in water quality from OWT1 to OWT3, a deviation of two classes is deemed highly significant, occurring in just 0.4% of cases (where OWT1 for OWT_{MER_OLCI} corresponds to OWT3 of OWT_{MODIS}).

Whether using the OWT_{MODIS} or the OWT_{MER_OLCI}, when there is an OWT2 assignment, in cases of disagreement between OWTs, such deviation is almost always in terms of underestimation. In other words, when a pixel is assigned OWT2 in one series, the adjacent pixel in the other series is often assigned OWT1 (and more rarely OWT3). This suggests not only that the OWT1 and OWT2 clusters show greater spectral similarity between them but also that the cluster representing the poorest water quality (OWT3) exhibits a significant distance from the OWT1 cluster.

3) Temporal Variability of OWT: Seasonal variation of OWTs is presented between 2003 and 2022 (see Fig. 7). Each subplot shows the frequency (in %) associated with each OWT cluster for each season.

The red color (OWT3) represents poorer water quality associated with high turbidity and with the presence of microalgae blooms. In Fig. 7, five subplots are presented. The top three represent OWT_{MER_OLCI} with the following modifications.

1) OWT_{MER_OLCI} with all available and coincident bands between MERIS and OLCI, ranging from 490 to 709 nm (300 m resolution).
2) Same as 1), but with spectral degradation, using only the bands coincident with MODIS (300 m resolution).
3) OWT_{MER_OLCI} with spatial resolution degradation for better similarity to MODIS resolution. Using the bands coincident with MODIS, adjacent pixels, and the same days to run the K-means method (900 m resolution).

Finally, two subplots are presented using the MODIS dataset.

4) OWT_{MODIS}, considering only the overlapping periods and adjacent pixels in relation to the MERIS and OLCI period (1000 m resolution).
5) OWT_{MODIS}, considering the complete 20-year period (1000 m resolution).

The transition from the first to the second subplot aims to verify differences in the OWTs obtained with a loss of the spectral information of these two sensors (MERIS and OLCI).
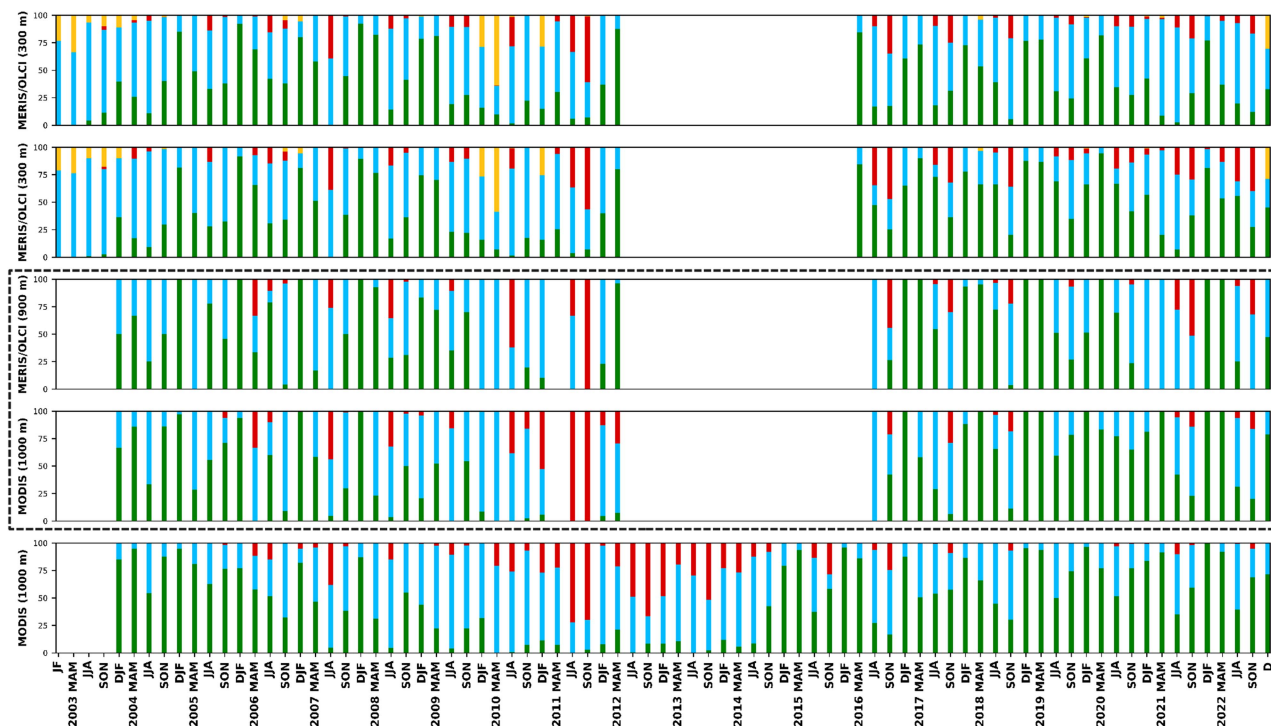
Fig. 7. Seasonal frequency (%) using the series initiated with the MERIS instrument and complemented with OLCI in the top three subplots. The second series has spectral degradation compared to the first subplot, and the third subplot is the same as the second but with spatial resolution degradation (from 300 to 900 m) and coincident with MODIS days. The two lower subplots represent the OWT_{MODIS}, for pixels consistent with OWT_{MER_OLCI} (second last subplot), and using the entire series available (last subplot).

The comparison from the second to the third aims to assess the change in OWT assignment when degrading the spatial resolution from 300 to 900 m. It is important to highlight that this degradation results in a shift in the optimal number of clusters, decreasing from four to three clusters, which aligns with the clusters assigned using the MODIS instrument. The dashed rectangle represents the two subplots for the direct comparison between the OWT_{MER_OLCI} and OWT_{MODIS} with 900 m resolution and 1000 m resolution, respectively. The transition from the fourth to the fifth subplot illustrates the variability in OWT assignments based on the sample used.

In essence, it demonstrates the results when applying the K-means clustering method, considering only the periods that overlap between sensors or using all available MODIS data.

In early 2003, during the filling phase following the closure of the gates in 2002, the Alqueva reservoir did not yet exhibit very low surface reflectances (OWT1) due to the agitation and mixing of water caused by this inflow (filling period). Starting from 2004, there has been a predominance of OWT1 during the colder water periods (DJF and MAM), while OWT2 and mainly OWT4 (the representative cluster of very turbid water) prevail in cases of runoff following intense precipitation events, being OWT4 only observed at a 300 m resolution. During periods of warmer water (JJA and SON), there are instances where clusters representing better water quality (OWT1 or OWT2) are assigned. However,

during the presence of microalgae blooms, there is a greater predominance of the OWT3 cluster.

The difference in OWT assignment between the two upper subplots (OWT_{MER_OLCI} at 300 m) is not significant, meaning that spectral degradation does not lead to relevant variations in OWT assignment on a seasonal basis for the period 2003–2022. The OWT4 to OWT_{MER_OLCI} (represented in yellow in Fig. 7) shows a significant distance from the average clusters of the other OWTs [see Fig. 6(b)]. For this reason, this cluster is identified in a very similar way using all available bands of the MERIS and OLCI instruments (upper subplot of Fig. 7) or with spectral degradation (second subplot from the top).

The use of a spatial resolution of 900 m instead of 300 m (for MERIS and OLCI) causes some significant variations.

1) The number of clusters decreases from four to three, with the cluster with extreme reflectances (OWT4) no longer existing. With a shorter distance between clusters and no representative cluster for highly turbid water due to runoff, the OWT assignment declines to the two closest clusters (OWT2 or OWT3).
2) An increased assignment to the OWT2 cluster, which has low reflectances but higher than OWT1.
3) An increase in the assignment to OWT3 (in red), where the proximity to the OWT2 cluster should be the main reason (see Fig. 6).

In the comparison of coincident pixels between OWT_{MER_OLCI} and OWT_{MODIS} (third and fourth subplots
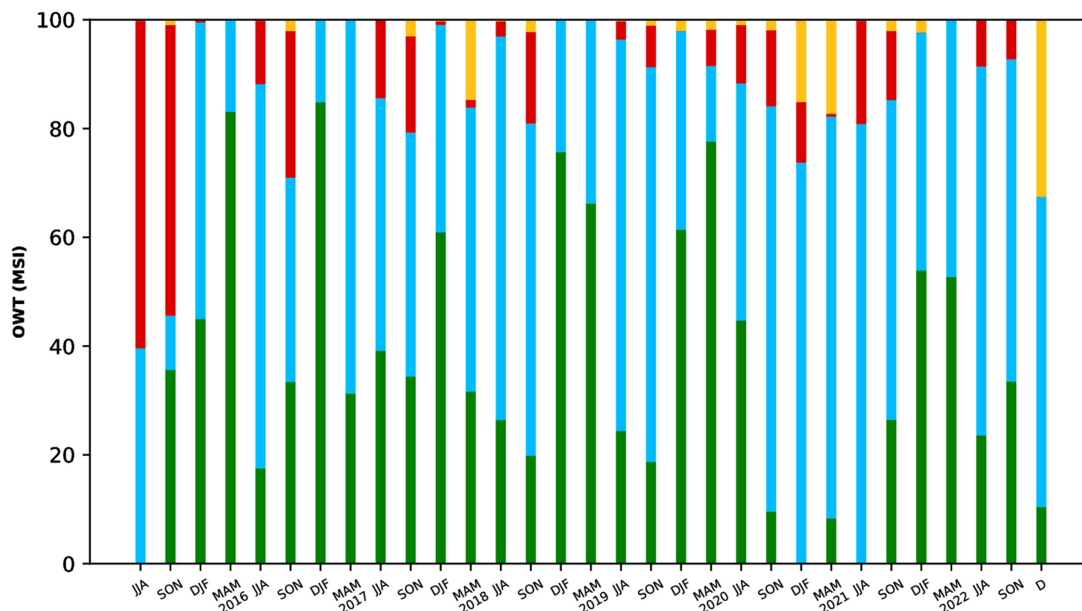
Fig. 8.   Seasonal frequency (%) of each of the OWTs for the period June 2015–2022 using the MSI instrument. The green bars represent OWT1, in blue is OWT2, in red is OWT3, and in yellow is OWT4.

in Fig. 7), there is a good similarity in the frequency of the three assigned clusters for most seasons of the year. However, in some seasons, there is an overestimation of OWT2 for OWT_{MER_OLCI} compared to MODIS, especially during seasons with a higher presence of microalgae, i.e., in the JJA and SON periods. For the MODIS instrument, by extending the sample period for the K-means run (fifth subplot compared to the fourth subplot in Fig. 7), there is an improvement in water quality during coincident periods.

The analysis of the seasonal evolution of OWT_{MER_OLCI} using a resolution of 300 m (with data gaps between June 2012 and March 2016) shows an increase in the OWT1 cluster in recent years, along with a growing predominance of OWT3 in the autumn, mostly associated with microalgae blooms. There is also a change in the patterns of microalgae blooms. From 2004 to 2011 (300 m resolution), microalgae blooms were more prevalent in the summer (JJA) compared to the autumn. However, from 2012 onwards, there has been a consistent increase in microalgae predominance in the autumn. This increase in autumnal microalgae prevalence in the last decade is also observed in broader regions when using spatial resolutions of 900 or 1000 m. In Fig. 8, the evolution of OWTs is presented using the MSI instrument from the Sentinel-2 mission.

V. DISCUSSION

The same atmospheric correction method (6SV code) was applied to data from all sensors to avoid introducing biases in the results. In the comparison between ESA sensors (MERIS, OLCI, and MSI) and MODIS, the bands that exhibit the largest deviations (in percentage terms) are the ones less influenced

by atmospheric correction, specifically the bands at 667 and 678 nm. However, it is important to consider that when water quality is good (high water transparency), surface reflectance is very low in this part of the spectrum. Therefore, even relatively small absolute errors can translate into relatively significant deviations in percentage terms. On the other hand, the green band, which plays a crucial role in monitoring microalgae blooms and chlorophyll-a concentrations, shows very low deviations (and similar deviations across sensors) and correlations very close to 1, as verified by Fig. 5 and Table II. The larger and deeper sections of the Alqueva reservoir show relatively minor spatial variations in water quality when compared to the narrower regions. The MODIS instrument, with a 1000-m resolution, only covers these broader areas. Consequently, when conducting statistical comparisons between MODIS and sensors with higher spatial resolutions such as MERIS, MSI, and OLCI, the deviations are quite similar, whether the nearest pixel (300 m) is used or averages of the reflectances from adjacent pixels (900 m).

The OWT classification scheme groups water quality based on the distinctive patterns observed in their reflectance spectra. These patterns are determined by the water's optical properties, which are influenced by the absorption and scattering of the water constituents. The application of the K-means method to almost the entire reservoir (MERIS and OLCI at 300 m spatial resolution) and subsequently only to broader areas (the same instruments at 900 m spatial resolution) results in a reduction in the number of ideal clusters for representing OWTs (Four to three). This fact underscores that in the broader areas of the reservoir, there is significantly less spatial variation in water quality when compared to the narrower areas. The OWT representative of the microalgae blooms has a higher representativeness

(percentage relative to other clusters) when using a 900-m resolution. This does not necessarily imply worse water quality (higher reflectances) in broader areas. Instead, it suggests that the cluster representing poorer water quality exhibits greater proximity to the midpoint of the other clusters making it easier to assign the OWT3 related to higher water turbidity. Note that there are moderate differences in the OWT_{MODIS} assignment when applying the clustering method over the entire 20-year period or only for the periods and pixels coinciding with OWT_{MER_OLCI} as verified by the seasonal variation shown in Fig. 7. This illustrates the significance of the sample used when applying the clustering method even when using the same satellite and wavelengths. If the objective is to intercompare different sensors for OWT assignment, it is essential to perform this analysis by applying the clustering method to colocated dates and pixels.

The Alqueva reservoir features significant depth in its wider areas, where the comparison between MODIS and other instruments is conducted. Here, water quality changes more gradually compared to the narrower and shallower regions. Consequently, a 1-h difference in satellite overpasses will have minimal impact on water quality and the subsequent statistical comparison. In this reservoir, most of the microalgae blooms that occur in the summer and early autumn begin to propagate from the northern region of the reservoir. Nevertheless, when utilizing the MODIS sensor, there are very few purely water pixels in this narrower zone of the reservoir throughout the 20-year period under analysis. As a result, a deterioration in water quality starting in the northern part of the reservoir can only be effectively identified with instruments such as MERIS, OLCI, or MSI. In a water reservoir that typically exhibits low surface reflectances, the spectral capacity of the sensor becomes crucial to identify these subtle differences. The limited spectral capacity of the MSI instrument to monitor water quality, due to large bandwidths, may explain the discrepancies in OWTs obtained for MSI and OLCI in the same analyzed seasons of the year. On the other hand, the substantial advantage of the MSI instrument, with its high spatial resolution of 10/20/60 m (depending on the band), in the Alqueva reservoir, may not be a factor of great relevance, considering that instruments with 300 m, such as MERIS and OLCI, already enable the analysis of narrower areas of the reservoir. The MSI instrument, however, can be crucial, being the only one among the four instruments analyzed that allows the analysis of variations in water quality in the Guadiana River (a narrow river in the area immediately upstream of the reservoir), which is the main water source north of the Alqueva reservoir.

Using the OWTs identified through the robust dataset from the MERIS and OLCI instruments, it becomes feasible to define OWTs in other reservoirs with similar characteristics employing methods such as Euclidean distance. To achieve this, the normalized reflectances of the study reservoir, where distinct OWTs are to be identified, should be compared with the average normalized reflectances of each cluster in the reference reservoir (Alqueva Reservoir), as shown in Fig. 10, for the OWT_{MER_OLCI} with a 300 m spatial resolution. It is important to note that the average

OWTs established in this study may not accurately represent reservoirs with small shallow reservoirs, or reservoirs characterized by extreme eutrophication (hypereutrophic) or very turbid water.

VI. CONCLUSION

Satellite remote sensing has proven to be a valuable tool for global water quality monitoring. This study aimed to compare water surface reflectances and OWTs in the Alqueva reservoir using four different sensors over two decades. Our results demonstrate that while all sensors provide useful data, medium-to-high spatial resolution sensors (MERIS, MSI, OLCI) are essential for accurately detecting runoff or microalgae blooms, particularly in narrower regions where broader coverage sensors, such as MODIS, may be less effective. MODIS, with its broader temporal coverage, provides a valuable reference for intersensor comparisons. Consistent atmospheric correction ensured reliable comparisons between sensors, and the green band exhibited the best statistical performance, making it an excellent indicator for long-term analysis of microalgae bloom trends in the Alqueva reservoir. The MERIS and OLCI instruments, with their excellent spectral resolution and sufficient spatial resolution for large reservoirs (300 m), provided a continuous and robust dataset, with a gap between April 2012 and March 2016 and were particularly well-suited for monitoring microalgae blooms.

A reservoir as large and deep as Alqueva has a greater capacity for attenuation and a slower response to the effects of climate change. Consequently, microalgae blooms in the Alqueva reservoir have not significantly increased during the summer in recent years, as shown by the seasonal analysis over the 20-year period. However, there has been an increase in blooms during the autumn (SON) period, likely linked to prolonged summers and unusually warm October months.

Most of the Alqueva reservoir exhibits high water transparency (OWT1/OWT2), with low surface reflectance and generally good water quality. Larger and deeper areas of the reservoir show less variability in water quality, while narrower regions are more vulnerable to fluctuations. By highlighting the differences between the spatial and spectral resolutions of the four instruments, this study contributes to the development of more efficient and accurate water quality monitoring systems.

It is important to note that the qualitative water quality classifications (OWTs defined for the distinct sensors) were not validated against in situ water quality parameters in this study. For future research, it is recommended to validate satellite estimates against quantitative water quality measurements, such as turbidity, water transparency, and chlorophyll-a concentrations. This validation would not only enhance the applicability of OWTs but also enable a more robust analysis of the trophic states identified in the Alqueva reservoir over time.
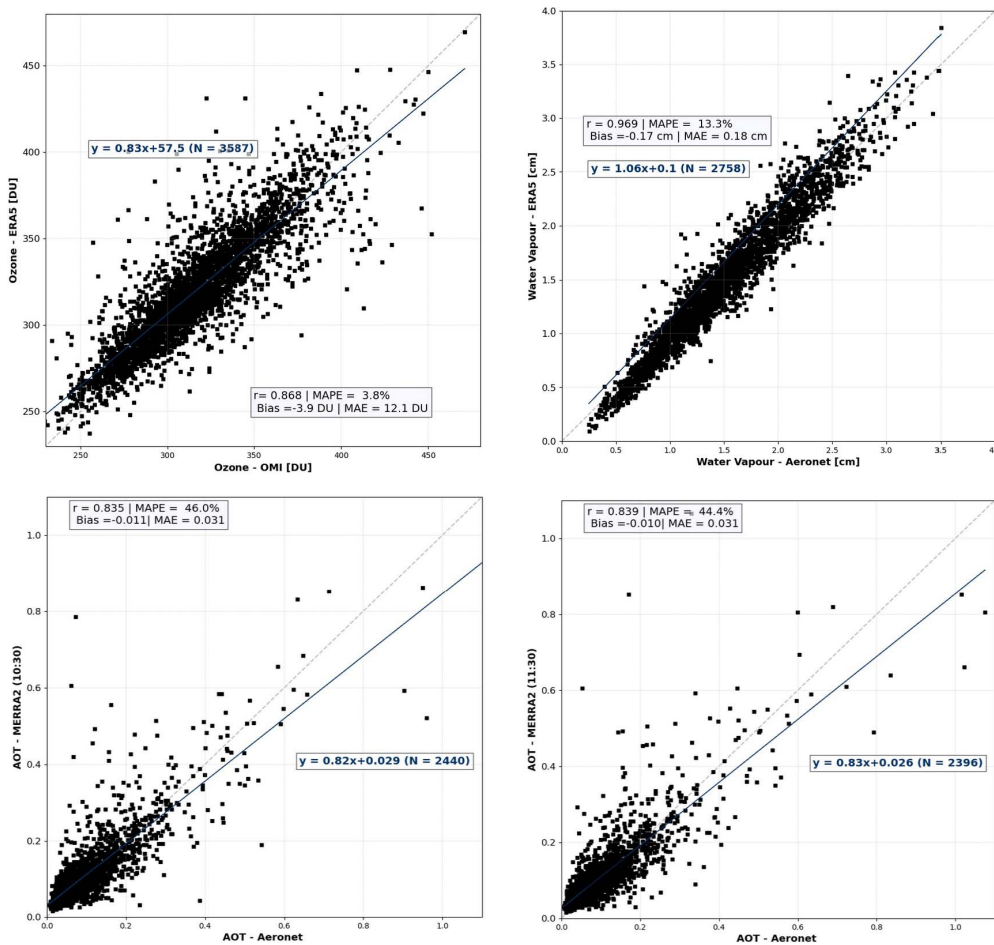
APPENDIX

Fig. 9.   Validation of the ozone and WV (upper panels) and AOT550 products for 10:30 and 11:30 time (lower panels).
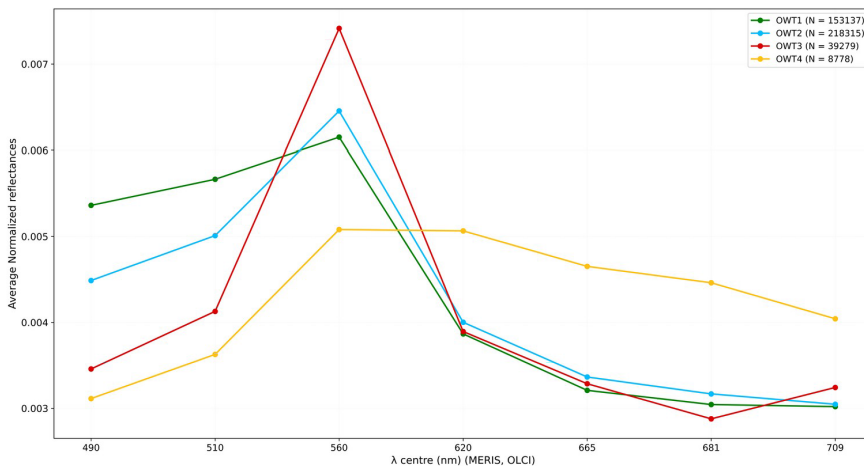

Fig. 10.   Reference reflectance normalized spectra used for OWT_{MER_OLCI} with a 300 m spatial resolution.

R<small>EFERENCES</small>

[1] R. M. Cardoso, P. M. M. Soares, D. C. A. Lima, and P. M. A. Miranda, "Mean and extreme temperatures in a warming climate: EURO CORDEX and WRF regional climate high-resolution projections for Portugal," *Climate Dyn.*, vol. 52, pp. 129–157, 2019, doi: 10.1007/s00382-018-4124-4.

[2] G. Meehl et al., *Global Climate Projections, Climate Change 2007: The Physical Science Basis*. Cambridge, U.K.: Cambridge Univ. Press, 2007, pp. 747–845.

[3] P. M. M. Soares, R. M. Cardoso, D. C. A. Lima, and P. M. A. Miranda, "Future precipitation in Portugal: High-resolution projections using WRF model and EURO-CORDEX multi-model ensembles," *Climate Dyn.*, vol. 49, pp. 2503–2530, 2017, doi: 10.1007/s00382-016-3455-2.

[4] S. Westra et al., "Future changes to the intensity and frequency of short-duration extreme rainfall," *Rev. Geophys.*, vol. 52, pp. 522–555, 2014, doi: 10.1002/2014RG000464.

[5] S. C. Palmer, T. Kutser, and P. D. Hunter, "Remote sensing of inland waters: Challenges, progress and future directions," *Remote Sens. Environ.*, vol. 157, pp. 1–8, 2015, doi: 10.1016/j.rse.2014.09.021.

[6] A. A. A. Saeid, "Remote sensing in water quality and water resources management," *Int. J. Res. Appl. Sci. Biotechnol.*, vol. 9, no. 1, pp. 163–170, 2022, doi: 10.31033/ijrasb.9.1.19.

[7] H. Yang, J. Kong, H. Hu, Y. Du, M. Gao, and F. Chen, "A review of remote sensing for water quality retrieval: Progress and challenges," *Remote Sens.*, vol. 14, 2022, Art. no. 1770, doi: 10.3390/rs14081770.

[8] H. Xi et al., "Satellite monitoring of surface phytoplankton functional types in the Atlantic Ocean over 20 years (2002–2021)," in *Copernicus Ocean State Report*, vol. 1, p. 5, 2023, doi: 10.5194/sp-2022-6.

[9] C. Giardino et al., "Evaluation of multi-resolution satellite sensors for assessing water quality and bottom depth of lake Garda," *Sensors*, vol. 14, pp. 24116–24131, 2014.

[10] X. Sòria-Perpinyà et al., "Validation of water quality monitoring algorithms for Sentinel-2 and Sentinel-3 in Mediterranean inland waters with in situ reflectance data," *Water*, vol. 13, 2021, Art. no. 686, doi: 10.3390/w13050686.

[11] S. N. Topp, T. M. Pavelsky, D. Jensen, M. Simard, and M. R. V. Ross, "Research trends in the use of remote sensing for inland water quality science: Moving towards multidisciplinary applications," *Water*, vol. 12, 2020, Art. no. 169, doi: 10.3390/w12010169.

[12] M. Potes et al., "Use of Sentinel 2-MSI for water quality monitoring at Alqueva reservoir, Portugal," *Proc. Int. Assoc. Hydrological Sci.*, vol. 380, pp. 73–79, 2018.

[13] K. Toming, T. Kutser, A. Laas, M. Sepp, B. Paavel, and T. Nõges, "First experiences in mapping lake water quality parameters with Sentinel-2 MSI imagery," *Remote Sens.*, vol. 8, 2016, Art. no. 640.

[14] C. D. Mobley, J. Werdell, B. Franz, Z. Ahmad, and S. Bailey, "Atmospheric correction for satellite ocean color radiometry," A Tutorial and Documentation of the Algorithms Used by the NASA Ocean Biology Processing Group, NASA, Greenbelt, MD, USA, 2016. [Online]. Available: https://ntrs.nasa.gov/api/citations/20160011399/downloads/20160011399.pdf

[15] K. Sørensen, E. Aas, and J. Høkedal, "Validation of MERIS water products and bio-optical relationships in the Skagerrak," *Int. J. Remote Sens.*, vol. 28, no. 3/4, pp. 555–568, 2007, doi: 10.1080/01431160600815566.

[16] M. Potes et al., "Lake-atmosphere interactions at Alqueva reservoir: A case study in the summer of 2014," *Tellus A, Dyn. Meteorol. Oceanogr.*, vol. 69, 2017, Art. no. 1272787.

[17] P. Palma, L. Ledo, S. Mesquita Soares, I. Barbosa, and P. Alvarenga, "Spatial and temporal variability of the water and sediments quality in the Alqueva reservoir (Guadiana Basin; Southern Portugal)," *Sci. Total Environ.*, vol. 470/471C, pp. 780–790, 2013, doi: 10.1016/j.scitotenv.2013.10.035.

[18] M. H. Novais, A. M. Penha, E. A. Morales, M. Potes, R. Salgado, and M. Morais, "Vertical distribution of benthic diatoms in a large reservoir (Alqueva, Southern Portugal) during thermal stratification," *Sci. Total Environ.*, vol. 659, pp. 1242–1255, 2019, doi: 10.1016/J.SCITOTENV.2018.12.251.

[19] G. Rodrigues, M. Potes, A. M. Penha, M. J. Costa, and M. M. Morais, "The use of Sentinel-3/OLCI for monitoring the water quality and optical water types in the largest Portuguese reservoir," *Remote Sens.*, vol. 14, no. 9, 2022, Art. no. 2172, doi: 10.3390/rs14092172.

[20] M. Morais, A. Serafim, P. Pinto, A. Ilhéu, and M. Ruivo, "Monitoring the water quality in Alqueva reservoir, Guadiana river, Southern Portugal," in *Reservoir and River Basin Management. Exchange of Experiences From Brazil, Portugal and Germany*, G. Gunkel and M. Sobral, Eds., Berlin, Germany: Universitätsverlag der TU Berlin Universitätsbibliothek Fasanenstr, 2007, pp. 96–112.

[21] P. Palma et al., "Evaluation of surface water quality using an eco-toxicological approach: A case study of the Alqueva reservoir (Portugal)," *Environ. Sci. Pollut. Res. Int.*, vol. 17, pp. 703–716, 2009, doi: 10.1007/s11356-009-0143-3.

[22] P. Palma, P. Alvarenga, V. L. Palma, R. M. Fernandes, A. M. Soares, and I. R. Barbosa, "Assessment of anthropogenic sources of water pollution using multivariate statistical techniques: A case study of the Alqueva's reservoir, Portugal," *Environ. Monit. Assessment*, vol. 165, no. 1/4, pp. 539–552, 2010.

[23] P. Palma, L. Ledo, S. Mesquita Soares, I. Barbosa, and P. Alvarenga, "Integrated environmental assessment of freshwater sediments: A chemical and ecotoxicological approach at the Alqueva reservoir," *Environ. Geochem. Health*, vol. 36, pp. 209–223, 2014, doi: 10.1007/s10653-013-9559-2.

[24] P. Palma, L. Ledo, and P. Alvarenga, "Assessment of trace element pollution and its environmental risk to freshwater sediments influenced by anthropogenic contributions: The case study of Alqueva reservoir (Guadiana Basin)," *Catena*, vol. 128, pp. 174–184, 2015, doi: 10.1016/j.catena.2015.02.002.

[25] P. Palma et al., "Water - sediment physicochemical dynamics in a large reservoir in the Mediterranean region under multiple stressors," *Water*, vol. 13, 2021, Art. no. 707.

[26] P. Palma et al., "Occurrence and risk assessment of pesticides in a Mediterranean Basin with strong agricultural pressure (Guadiana Basin: Southern of Portugal)," *Sci. Total Environ.*, vol. 794, 2021, Art. no. 148703, doi: 10.1016/j.scitotenv.2021.148703.

[27] A. Penha, A. Chambel, M. Murteira, and M. Morais, "Influence of different land uses on groundwater quality in southern Portugal," *Environ. Earth Sci.*, vol. 75, 2016, Art. no. 622, doi: 10.1007/s12665-015-5038-7.

[28] M. Potes, M. J. Costa, R. Salgado, D. Bortoli, A. Serafim, and P. Le Moigne, "Spectral measurements of underwater downwelling radiance of inland water bodies," *Tellus-A*, vol. 65, 2013, Art. no. 20774, doi: 10.3402/tellusa.v65i0.20774.

[29] V. H. Neves, G. Pace, J. Delegido, and S. C. Antunes, "Chlorophyll and suspended solids estimation in Portuguese reservoirs (Aguieira and Alqueva) from Sentinel-2 imagery," *Water*, vol. 13, no. 18, 2021, Art. no. 2479, doi: 10.3390/w13182479.

[30] M. Potes, M. J. Costa, J. C. B. da Silva, A. M. Silva, and M. Morais, "Remote sensing of water quality parameters over alqueva reservoir in the South of Portugal," *Int. J. Remote Sens.*, vol. 32, pp. 3373–3388, 2011, doi: 10.1080/01431161003747513.

[31] M. Potes, M. J. Costa, and R. Salgado, "Satellite remote sensing of water turbidity in Alqueva reservoir and implications on lake modelling," *Hydrol. Earth Syst. Sci.*, vol. 16, pp. 1623–1633, 2012.

[32] G. Rodrigues et al., "Temporal and spatial variations of secchi depth and diffuse attenuation coefficient from Sentinel-2 MSI over a large reservoir," *Remote Sens.*, vol. 12, no. 5, 2020, Art. no. 768, doi: 10.3390/rs12050768.

[33] A. Silva, I. De Lima, F. Santo, and V. Pires, "Assessing changes in drought and wetness episodes in drainage basins using the standardized precipitation index," *Bodenkultur*, vol. 65, no. 3/4, pp. 31–37, 2014.

[34] V. V. Salomonson, W. L. Barnes, P. W. Maymon, H. E. Montgomery, and H. Ostrow, "MODIS: Advanced facility instrument for studies of the Earth," *IEEE Trans. Geosci. Remote Sens.*, vol. 27, no. 2, pp. 145–153, Mar. 1989.

[35] ESA, "MERIS product handbook. Issue 2.0," 2006, Accessed: Dec. 2023. [Online]. Available: http://envisat.esa.int/handbooks/meris/

[36] A. Detoni, G. Navarro, J. Garrido, F. Rodríguez, J. Hernández-U., and I. Caballero, "Mapping dinoflagellate blooms (Noctiluca and Alexandrium) in aquaculture production areas in the NW Iberian Peninsula with the Sentinel-2/3 satellites," *Sci. Total Environ.*, vol. 868, 2023, Art. no. 161579, doi: 10.1016/j.scitotenv.2023.161579.

[37] S. Bailey and J. Werdell, "A multi-sensor approach for the on-orbit validation of ocean color satellite data products," *Remote Sens. Environ.*, vol. 102, pp. 12–23, 2006, doi: 10.1016/j.rse.2006.01.015.

[38] C. Hu, Z. Lee, and B. Franz, "Chlorophyll a algorithms for oligotrophic oceans: A novel approach based on three-band reflectance difference," *J. Geophysical Res.*, vol. 117, 2012, Art. no. C01011, doi: 10.1029/2011JC007395.

[39] W. Moutier, S. J. Thomalla, S. Bernard, G. Wind, T. J. Ryan-Keogh, and M. E. Smith, "Evaluation of chlorophyll-a and POC MODIS aqua products in the Southern Ocean," *Remote Sens.*, vol. 11, no. 15, 2019, Art. no. 1793, doi: 10.3390/rs11151793.

[40] M. Á. Obregón, G. Rodrigues, M. J. Costa, M. Potes, and A. M. Silva, "Validation of ESA Sentinel-2 L2A aerosol optical thickness and columnar

water vapour during 2017–2018," *Remote Sens.*, vol. 11, no. 14, 2019, Art. no. 1649, doi: 10.3390/rs11141649.

[41] V. Salgueiro et al., "Characterization of Tajogaite volcanic plumes detected over the Iberian Peninsula from a set of satellite and ground-based remote sensing instrumentation," *Remote Sens. Environ.*, vol. 295, 2023, Art. no. 113684, doi: 10.1016/j.rse.2023.113684.

[42] C. Gueymard and D. Yang, "Worldwide validation of CAMS and MERRA-2 reanalysis aerosol optical depth products using 15 years of AERONET observations," *Atmos. Environ.*, vol. 225, 2019, Art. no. 117216, doi: 10.1016/j.atmosenv.2019.117216.

[43] ASD, *FieldSpec HandHeld 2 Spectroradiometer User's Manual*, vol. 1. Boulder, CO, USA: ASD, 2010, pp. 1–93.

[44] E. J. Botha, J. M. Anstee, S. Sagar, E. Lehmann, and T. A. G. Medeiros, "Classification of Australian waterbodies across a wide range of optical water types," *Remote Sens.*, vol. 12, 2020, Art. no. 3018.

[45] E. Spyrakos et al., "Optical types of inland and coastal waters," *Limnol. Oceanogr.*, vol. 63, pp. 846–870, 2018.

[46] Z. Huang, "Extensions to the K-means algorithm for clustering large data sets with categorical values," *Data Mining Knowl. Discov.*, vol. 2, pp. 283–304, 1998.

[47] V. Vantrepotte, H. Loisel, D. Dessailly, and X. Mériaux, "Optical classification of contrasted coastal waters," *Remote Sens. Environ.*, vol. 123, pp. 306–323, 2012.

[48] P. J. Rousseeuw, "Silhouettes: A graphical aid to the interpretation and validation of cluster analysis," *J. Comput. Appl. Math.*, vol. 20, pp. 53–65, 1987.

Gonçalo Rodrigues received the integrated master's degree in energy and environmental engineering from the Faculty of Sciences, University of Lisbon, Lisbon, Portugal, in 2014. After contributing to nowcasting systems and fire weather index sensitivity studies with the Portuguese Institute for Sea and Atmosphere, he is currently working toward the Ph.D. degree in Earth and space sciences from the University of Évora, Évora, Portugal.

His doctoral research focuses on fog detection and monitoring, as well as satellite-based water quality monitoring, including atmospheric correction and modeling techniques. His work involves quantifying parameters such as chlorophyll-a and water turbidity to assess water quality, while optical water types are used qualitatively to analyze algae bloom dynamics.

Miguel Potes received the graduate degree in meteorology, oceanography, and geophysics from the Faculty of Sciences, University of Lisbon, Lisbon, Portugal, in 2006 and the master's and Ph.D. degrees from Évora University, Évora, Portugal, in 2008 and 2013, respectively.

Since April 2023, he has been an Assistant Researcher with Universidade de Évora, Évora. He has solid knowledge of the physics of atmosphere and climate. His main research interests include meteorology, climate, hydrology, water quality, lakes, and watersheds.

Maria João Costa received the Ph.D. degree in physics in 2004 and the Habilitation in atmospheric and climate physics in 2020 from the University of Évora, Évora, Portugal.

She is a Full Professor with the Department of Physics, University of Évora, Évora. She is the Scientific Coordinator of the Center for Sci-Tech Research in Earth System and Energy. Her main research interests concern atmospheric physics, air and water quality, remote sensing, solar radiation, and atmospheric radiative transfer.